

Kinetic Roughening of Penetrating Flux Fronts in High- T_c Thin Film Superconductors

R. Surdeanu, R. J. Wijngaarden, E. Visser, J. M. Huijbregtse, J. H. Rector, B. Dam, and R. Griessen

*Division of Physics and Astronomy, Faculty of Sciences, Vrije Universiteit, De Boelelaan 1081,
1081 HV Amsterdam, The Netherlands*

(Received 7 December 1998)

Kinetic roughening of flux fronts penetrating in superconducting thin films are studied by means of a high resolution magneto-optic technique. The roughening exponent ($\alpha = 0.64$) and growth exponent ($\beta = 0.65$) obtained from a dynamic scaling analysis of the initial stage of flux penetration and, at small length scales, are characteristic for a static disorder dominated nonlinear diffusion such as also observed in the directed percolated depinning model. At large length scale, $\alpha = 0.46$ indicates a transition towards dynamic stochastic disorder, similar to the behavior of Kardar-Parisi-Zhang systems. There is a striking similarity with the behavior of combustion fronts in burning paper.

PACS numbers: 74.60.Ge, 68.35.Fx

The relevance of dynamic scaling concepts in the study of the growth of rough interfaces was illustrated in recent years by comprehensive theoretical and experimental work [1–5]. The interest is roused by the wide range of phenomena where roughening occurs: fluid flow in porous media [3,6–8], propagation of flame fronts in forest fires and in paper [9–11], deposition processes [2,4], bacterial growth [2], and tumor growth [12]. It has been proposed that the gradual thermal depinning of a single vortex line in a superconductor with randomly distributed weak pinning centers might exhibit increased roughening [2]. Gilchrist and van der Beek also suggested a similarity between transport in porous media and the nonlinear diffusion of vortices in hard superconductors [13,14]. This work stimulated us to search for kinetic roughening effects in high- T_c superconducting thin films with a tailored defect structure leading to strong pinning. From a detailed magneto-optical investigation of flux penetration fronts in films, we made the interesting discovery that penetrating flux fronts exhibit the same roughening and growth behavior as burning paper [9–11].

The samples used for this work are $\text{YBa}_2\text{Cu}_3\text{O}_{7-x}$ films on NdGaO_3 substrates [15,16]. The film thickness is only 80 nm to prevent strain in the film. Analysis with Rutherford backscattering spectrometry and x-ray indicates that the a and b axes have the same orientation over the whole film, while the c axis is perpendicular to the substrate. The good quality of the films is also confirmed by the high critical current density of $1.2 \times 10^{11} \text{ A m}^{-2}$ at 4.2 K in 0 T. The T_c of the films is 90 K, with a $\Delta T_c = 0.5$ K. The thin films are patterned, using standard photolithography, in stripes with an aspect ratio of 1:9 in the a - b plane, the long edge having a dimension of 8.1 mm. Only the middle part of the long edges is used to eliminate the finite size effects on the shape of the fronts at the corners. The studied edges of the samples were patterned as a straight line for sample No. 1 and with a zigzag pattern of 1 μm tooth width for sample No. 2. Results for both samples are the same as discussed below,

which indicates that the observed behavior is not sensitive to edge topology.

The magneto-optic (MO) experiments are performed using Bi-doped YIG films with in-plane anisotropy as an indicator for the local magnetic field. The spatial resolution of the indicator is better than 1 μm . The indicator is placed on top of the sample, and the ensemble is mounted in our specially designed cryogenic polarization microscope which fits into the variable temperature insert of an Oxford instruments 1-T magnet system. This setup creates a two-dimensional image of the local magnetic field at the surface of the sample. The sample is cooled in zero field to 4.2 K. Subsequently, the magnetic field is applied parallel to the c axis of the sample, and images are recorded at 1 mT intervals. From the MO image, the flux front is determined as the borderline between the Shubnikov region where vortices are present (high intensity in the MO image) and the flux-free (Meissner) region (low intensity). At this borderline, by definition, the local intensity equals the background intensity plus 3 times the standard deviation of the noise in the background intensity. The magnification is such that a pixel corresponds to 3 μm , much larger than the largest details (growth islands of 200 nm diameter) of the sample microstructure. Figure 1a shows a false-color MO image (high intensity represented with yellow, low intensity with blue) of sample No. 2 at 11 mT. The image shows only the part used for the analysis. The edge of the sample is indicated by the black dotted line. The wiggly white line is added to indicate the determined flux front. Figure 1b illustrates flux fronts taken at a 1 mT interval from 1 to 17 mT. Since the average of the flux front progresses linearly with field, the value of the external field is also indicative of the time at which a front is recorded (the vortex diffusion is driven by the external field). The deviation from linear progression due to the thin film geometry is taken into account.

The analysis of the front scaling behavior is performed by means of two methods.

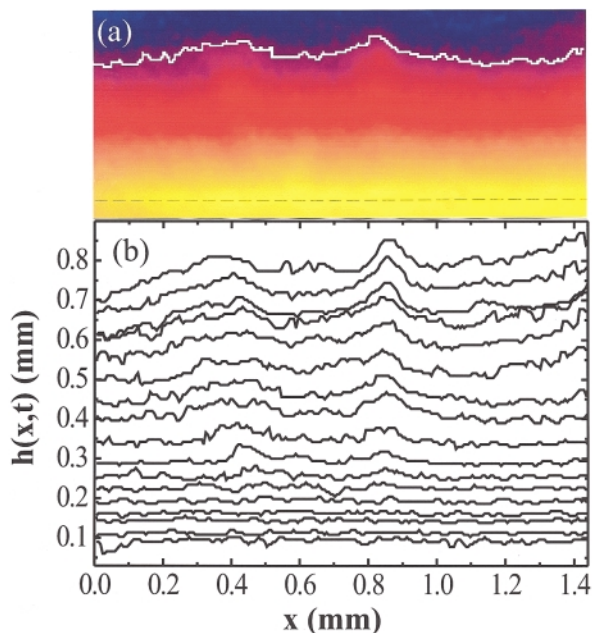


FIG. 1. (a) (color) Magneto-optical image taken at 11 mT after zero field cooling to 4.2 K of a 80 nm thick $\text{YBa}_2\text{Cu}_3\text{O}_{7-x}$ film on NdGaO_3 (sample No. 2). High vortex density is represented with yellow and low vortex density with blue. The image shows only the part used for analysis (1.44 mm in length) and the wiggly white line indicates the flux front (determined according to the procedure described in the text). The total length of the sample is 8.1 mm. (b) Flux fronts observed in sample No. 2. The applied external field is increased by 1 mT between subsequent fronts. The first front (bottom) is recorded at 1 mT and the last one (top) at 17 mT.

(i) The interface width [2] $w(L, t) \equiv \sqrt{\langle [h(x, t) - \bar{h}(t)]^2 \rangle}$, which characterizes the roughness of the interface, is used: Here, x is the horizontal position and t is the time; the overbar denotes a spatial average over a width L . In the initial stage of the process, w scales as t^β while, in the saturation regime, w scales as L^α , where L is the system size. Although conceptually simpler, for our experiments, just as for the paper burning experiments [10], this approach is somewhat problematic for the calculation of β because of the rather rapid saturation of $w(t)$. The calculation of α was, however, possible due to the fairly large size of our systems, up to 500 pixels.

(ii) The two-point correlation function [2],

$$C(x, t) = \{[\delta h(x_0, t_0) - \delta h(x_0 + x, t_0 + t)]^2\}_{x,t}^{1/2}, \quad (1)$$

where $\delta h \equiv h - \bar{h}$ is also used. This quantity enables us to determine independently the exponents α and β by fitting

$$C(l, 0) \sim l^\alpha, \quad \text{for } l \ll l_{\text{sat}}, \quad (2)$$

$$C(0, t) \sim t^\beta, \quad \text{for } t \ll t_{\text{sat}}. \quad (3)$$

The algorithms were checked by applying them to ballistic deposition model and Eden model simulations,

which gave values for α and β in very good agreement with the literature [2].

Before applying the analysis, we corrected for the overall slope in the fronts' data. Figure 2 shows the spatial correlation function $[C(l, 0)]^2$ for the samples No. 1 and No. 2. It is immediately visible that both samples exhibit the same two distinct scaling regimes although sample No. 1 has straight edges while sample No. 2 has zigzag edges of $1\text{-}\mu\text{m}$ amplitude. At short length scales (regime I) the roughness exponent is $\alpha = 0.64$, while $\alpha = 0.46$ is found at larger length scales (regime II). These values are very close to those of the directed percolation depinning (DPD) model [2,3] in the case of a pinned interface and the Kardar-Parisi-Zhang (KPZ) [1,2] models, respectively.

To determine experimentally the growth exponent β , we calculate the time-dependent correlation function, $C(0, t)$. The graph representing $[C(0, t)]^2$ for both samples is shown in Fig. 3. As clearly seen in this figure, the curves scale with an exponent $\beta = 0.65$, in excellent agreement with the value given by the DPD model.

Remarkably, in experiments on burning paper [11], the same two regimes for $C(l, 0)$ with the same exponents were found. We now discuss the origin of this two regime behavior.

Simulations of the DPD model, which incorporate interface growth in the presence of *quenched* disorder, lead to $\alpha = 2/3$ [2] while the KPZ model, which is based on the nonlinear differential equation

$$\frac{\partial h(\vec{r}, t)}{\partial t} = \nu \nabla^2 h(\vec{r}, t) + \frac{\lambda}{2} [\nabla h(\vec{r}, t)]^2 + \eta(\vec{r}, t), \quad (4)$$

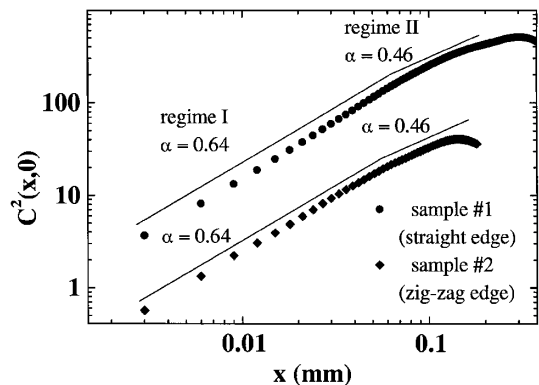


FIG. 2. Spatial correlation function calculated according to Eq. (1) for samples No. 1 and No. 2. Sample No. 1 has a straight edge, while the edge of sample No. 2 is patterned with a zigzag pattern of $1\text{-}\mu\text{m}$ tooth width. For clarity, the curves are shifted vertically by one decade. By definition, half of the slope in the log-log plot is the roughening exponent α . Values for both samples and for both regimes are indicated. Relatively high values close to the DPD value $\alpha = 2/3$ are observed for short lengths while, for large length scales, small values (close to the KPZ value $\alpha = 1/2$) are observed. The fact that the same exponents are obtained for a sample (No. 1) with a smooth edge and a sample (No. 2) with a zigzag edge proves that the edge topology is not relevant.

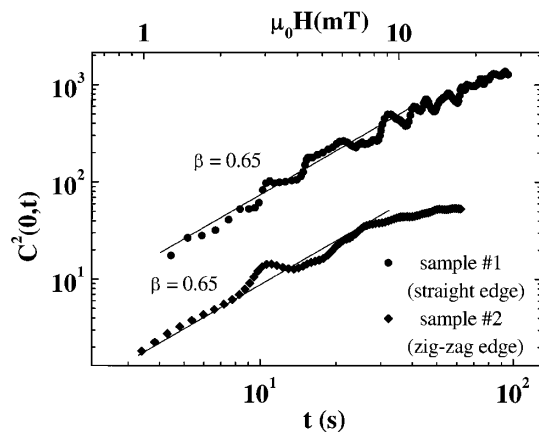


FIG. 3. Time-dependent correlation function for samples No. 1 and No. 2. Sample No. 1 has a straight edge, while the edge of sample No. 2 is patterned with a zigzag pattern of $1\text{-}\mu\text{m}$ tooth width. Since the average of the flux front progresses linearly with field, the value of the external field (shown on the upper x -axis) is also indicative of the time (shown on the lower x -axis) at which a front is recorded (the vortex diffusion is driven by the external field). The deviation from linear progression due to the thin film geometry is taken into account. Half of the slope of this log-log plot is the growth exponent β . Note that these values are close to the DPD value ($\beta = 2/3$) characteristic of static disorder.

leads to $\alpha = 1/2$. In Eq. (4), $h(\vec{r}, t)$ is the height of the advancing interface, ν and λ are constants, and $\eta(r, t)$ represents spatiotemporal disorder. The first term causes relaxation of the interface by the surface tension ν , while the second term tends to enhance irregularities. It is the lowest-order nonlinear term consistent with symmetries and conservation laws. Equation (4) was originally proposed by Kardar-Parisi-Zhang with a white noise function $\eta(\vec{r}, t)$, although it is noted that the actual form of the noise distribution is irrelevant. The KPZ model has a growth exponent $\beta = 1/3$, while the DPD model, on the other hand, is characterized by $\beta = 2/3$. From this we conclude that the crossover observed both in our experiments and that of Maunuksela *et al.* [10] may be caused by a crossover from DPD to KPZ behavior. This crossover occurs when temporal disorder starts to dominate the spatial disorder due to the sample microstructure. Indeed, for burning paper, Amaral and Makse [11] showed that the crossover in the roughness exponent occurs at a length scale related to (but not necessarily equal to) the correlation length of the disorder in the medium [11]. In our experiments we purposely took a larger pixel size than the length scale of the microstructure of the sample (island size), thus avoiding trivial effects due to “imaging” of the sample microstructure. Our scaling results show self-organization at much larger length scales than the static disorder in the system, but still dominated by it due to the relatively small temporal disorder. In other experiments we found that the crossover between

the two scaling regimes takes place at different values of x , suggesting that the crossover length is due to differences in the pinning landscape for vortices. Indeed, Dam *et al.* [17] demonstrated recently that the average separation of the linear defects responsible for strong pinning in $\text{YBa}_2\text{Cu}_3\text{O}_{7-x}$ films can be varied at will between 100 and 500 nm in pulsed laser deposited (PLD) films. These strong pinning linear defects occur at the merging of the trenches which separate growth islands. The effect is increased pinning and not the creation of weak links.

At large length scales, the cumulative effect of temporal disorder becomes dominant and exponents similar to the temporal fluctuations KPZ model are found. It is also relevant that in this regime, for repeated experiments, although the values for the exponents are precisely recovered, the shape of the front does not reproduce exactly. This is again indicative of a stochastic temporal disorder.

At this point it is interesting to ask ourselves why there is a strong similarity between burning paper (which exhibits, for certain regimes, KPZ behavior [10]) and flux penetration fronts in a superconductor. A partial answer to this question can be given by considering an activated model for vortex motion in a superconductor. From Maxwell’s relation $\nabla \times \vec{E} = -\frac{\partial \vec{B}}{\partial t}$ and $\vec{E} = \vec{B} \times \vec{v}$, which for thermally activated motion in one dimension can be written as $\vec{E} = \rho(j)\vec{j} = \rho_f \vec{j} e^{-U(j)/kT}$, where $\rho(j)$ is the current dependent resistivity, ρ_f is the flux-flow resistivity, and $U(j)$ is the current-dependent activation energy for vortex hopping, one can derive the following nonlinear equation:

$$\frac{\partial \rho(\vec{r}, t)}{\partial t} = \rho a(j) \frac{\partial^2 \rho(\vec{r}, t)}{\partial x^2} + b(j) \left[\frac{\partial \rho(\vec{r}, t)}{\partial x} \right]^2. \quad (5)$$

If a and b were constant, this would be the porous medium equation, which is similar to the KPZ equation, Eq. (4). The coefficients $a(j)$ and $b(j)$ depend in fact only weakly on the form of $U = U(j)$. They can be expressed in terms of the dynamical relaxation rate Q as $a(j) = (1 + 1/Q)$ and $b(j) = Q + dQ/d \ln j$. The dynamical relaxation rate $Q \equiv d \ln j / d \ln(\frac{\partial B}{\partial t})$ determined from the sweep rate dependence of the superconducting current is typically 0.03 ± 0.01 (see [18]) at low temperatures, and $dQ/d \ln j$ is usually very small [18]. Hence we approximately recover the porous medium equation (where a and b are constant). For the particular case of a logarithmic barrier dependence, i.e., $U(j) = U_0 \ln \frac{j}{j_c}$, we find $a = (1 + U_0/kT)$ and $b = kT/U_0$, that is, the porous medium equation as obtained by Gilchrist [14] is recovered exactly. From this we conclude that the resistivity obeys a nonlinear diffusion equation which is very similar to the porous medium equation, independent of the exact model used to describe the creep, i.e., the expression for $U(j)$. At this point it is important to mention that we do not study free diffusion, but driven diffusion of vortices in the presence of a field gradient.

Our experiment is similar to the driven diffusion of a wetting fluid in a porous medium consisting of glass beads closely packed between two glass plates [7].

The exact relation between the “porous medium” behavior of ρ and the measured development of the flux front is presently not clear and certainly deserves further theoretical investigation. It may, of course, be expected that the nonlinear behavior of ρ will result in lowest order in a KPZ equation for the flux front since the KPZ equation is the simplest nonlinear diffusion equation. The noise term $\eta(\vec{r}, t)$ in our case results both from static disorder and from thermal fluctuations, as discussed above.

In conclusion, our sensitive magneto-optical study of penetrating flux in superconducting thin films reveals kinetic roughening of the interface between the magnetic flux front and the vortex-free Meissner region. Two scaling regimes are found: At small length scales or short times where static disorder dominates, DPD-like exponents are found ($\alpha = 0.64$ and $\beta = 0.65$) while, at large length scales, temporal stochastic noise dominates and KPZ-like exponents are found ($\alpha = 0.46$). The main result of this Letter is that there is a striking analogy between our data on superconductors and the results obtained on burning paper fronts by Maunuksela *et al.* [10,11]. This suggests that vortex matter can be used as a model substance to explore nonlinear diffusion. For future studies vortex matter offers many advantages: (i) The density of particles is easily varied over a wide range by applying an external magnetic field; (ii) the dynamics of the system is much faster than that of many other systems; (iii) the driving force for diffusion is the external magnetic field or electric current, which can be both easily varied and controlled; (iv) the particle-particle (vortex-vortex) interaction is well known; (v) experiments with diffusion of positive particles (vortices) and negative particles (antivortices) in the same sample are possible; (vi) the experiments can be repeated many times on the same sample as the substrate is not destroyed; (vii) it has real physical interest (fractal penetration is unwanted in superconducting devices); (viii) in similar samples roughening can be easily tuned by changing the anisotropy in the critical current [16]. Conversely, the study of roughening in superconductors is intrinsically important as the scaling exponents are related to the nature of the noise in the system and are thus a sort of fingerprint

of the pinning landscape of the superconductor. To investigate this relation, high- T_c superconducting films are especially interesting since they can be synthesized with a tailored defect structure [17]. Work along these lines is in progress.

-
- [1] M. Kardar, G. Parisi, and Y.-C. Zhang, *Phys. Rev. Lett.* **56**, 889 (1986).
 - [2] A.-L. Barabási and H.E. Stanley, *Fractal Concepts in Surface Growth* (Cambridge University Press, Cambridge, UK, 1995).
 - [3] *Dynamics of Fractal Surfaces*, edited by F. Family and T. Vicsek (World Scientific, Singapore, 1991).
 - [4] T. Halpin Healy and Y.-C. Zhang, *Phys. Rep.* **254**, 215 (1995).
 - [5] L.A.N. Amaral, A.-L. Barabási, H.A. Makse, and H.E. Stanley, *Phys. Rev. E* **52**, 4087 (1995).
 - [6] S. He, G.L.M.K.S. Kahanda, and P.-z. Wong, *Phys. Rev. Lett.* **69**, 3731 (1992).
 - [7] M.A. Rubio, C.A. Edwards, A. Dougherty, and J.P. Gollub, *Phys. Rev. Lett.* **63**, 1685 (1989).
 - [8] J.P. Stokes, A.P. Kushnick, and M.O. Robbins, *Phys. Rev. Lett.* **60**, 1386 (1988).
 - [9] J. Zhang, Y.-C. Zhang, P. Alstrom, and M.T. Levinsen, *Physica (Amsterdam)* **189A**, 383 (1992).
 - [10] J. Maunuksela, M. Myllys, O.-P. Kähkönen, J. Timonen, N. Provatas, M.J. Alava, and T. Ala-Nissila, *Phys. Rev. Lett.* **79**, 1515 (1997).
 - [11] L.A.N. Amaral and H.A. Makse, *Phys. Rev. Lett.* **80**, 5706 (1998).
 - [12] A. Brú, J.M. Pastor, I. Feraud, I. Brú, S. Melle, and C. Berenguer, *Phys. Rev. Lett.* **81**, 4008 (1998).
 - [13] J. Gilchrist and C.J. van der Beek, *Physica (Amsterdam)* **231C**, 147 (1994).
 - [14] J. Gilchrist, *Physica (Amsterdam)* **291C**, 132 (1997).
 - [15] B. Dam, J. Rector, M.F. Chang, S. Kars, D.G. de Groot, and R. Griessen, *Appl. Phys. Lett.* **65**, 1581 (1994).
 - [16] R. Surdeanu, R.J. Wijngaarden, B. Dam, J. Rector, R. Griessen, C. Rossel, Z.F. Ren, and J.H. Wang, *Phys. Rev. B* **58**, 12467 (1998).
 - [17] B. Dam, J.M. Huijbregtse, F.C. Klaassen, R.C.F. van der Geest, G. Doornbos, J.H. Rector, A.M. Testa, S. Freisem, J. Aarts, J.C. Martínez, B. Stäubli-Pümpin, and R. Griessen, *Nature (London)* **399**, 439 (1999).
 - [18] A.J.J. van Dalen, M.R. Koblischka, and R. Griessen, *Physica (Amsterdam)* **259C**, 157 (1996).